Applied Surface Science 433 (2018) 829–835

Contents lists available at ScienceDirect

Applied Surface Science

journal homepage: www.elsevier.com/locate/apsusc

Full Length Article

Matrix coatings based on anodic alumina with carbon nanostructures in the pores

G.G. Gorokh[a,*], M.I. Pashechko[b], J.T. Borc[b], A.A. Lozovenko[a], I.A. Kashko[a], A.I. Latos[b]

[a] Belarusian State University of Informatics and Radioelectronics, Minsk, 220013, Belarus
[b] Lublin University of Technology, Lublin, 20-618, Poland

ARTICLE INFO

Article history:
Received 26 July 2017
Received in revised form 3 October 2017
Accepted 16 October 2017
Available online 18 October 2017

Keywords:
Nanoporous anodic alumina
Carbon nanostructure
Strengthening coatings
Friction coefficient

ABSTRACT

The nanoporous anodic alumina matrixes thickness of 1.5 mm and pore sizes of 45, 90 and 145 nm were formed on Si substrates. The tubular carbon nanostructures were synthesized into the matrixes pores by pyrolysis of fluid hydrocarbon xylene with 1% ferrocene. The structure and composition of the matrix coatings were examined by scanning electron microscopy, Auger analysis and Raman spectroscopy. The carbon nanostructures completely filled the pores of templates and uniformly covered the tops. The structure of carbon nanostructures corresponded to the structure of multiwall carbon nanotubes. Investigations of mechanical and tribological properties of nanostructured oxide-carbon composite performed by scratching and nanoindentation showed nonlinear dependencies of the frictional force, penetration depth of the cantilever, hardness and plane strain modulus on the load. It was found that the microhardness of the samples increases with reduced of alumina pore diameter, and the penetration depth of the cantilever into the film grows with carbon nanostructures size. The results showed the high mechanical strength of nanostructured oxide-carbon composite.

1. Introduction

The use of the inorganic nanoscale particles and structures dispersed in a matrix can significantly improve the strength and durability of materials. The mechanical and tribological characteristics of the materials coated with matrix film increase in several times [1]. In addition, such matrix nanocomposites exhibit high ablation resistance, which opens the perspective for their use to protect the surface of products from exposure to high temperatures. Recent studies testify to the very promising directions in the development of structural materials as well as nanostructured thin film matrixes filled with carbon containing nanoparticles [2]. The formation during friction (tribosynthesis) of the secondary structures based on C, B and Si with dimensions of the order of nanometers allows to increase wear resistance of the eutectic coatings based on systems Fe-Mn-C-B [3].

In order to tailor the properties of structural materials and thin film matrix, it is necessary to create an array with tunable size, shape, and spacing of regularly ordered carbon nanostructures (CNS), using patterning techniques. The most widespread way of orientation and location of CNS array is using of nanoporous templates [4] such as self-organized matrix films of porous anodic alumina (PAA) [5,6], which has a unique periodic cellular porous structure (a bee honeycomb structure); its parameters (pore size and number) can be controllably varied greatly from 10 to 400 nm and from 10^{12} to 10^{8} cm^{-2}, respectively, by changing the anodizing conditions.

The arrays of carbon nanotubes were successfully synthesized in PAA matrices, in which the unique electrophysical properties of nanotubes were used [7]. At the same time, such nanostructured system has high chemical resistance, high strength, rigidity, toughness, and thermal conductivity and it is assumed that new composite reinforcement coatings can be obtained on this model basis. It is important to obtain a uniform filling of the pores up to the edge of the output on PAA surface. This paper presents the results of the formation of oxide-carbon composite coatings on the basis of thin matrix of anodic alumina, in which pores are filled from the bottom to the surface with tubular carbon nanostructures, as well as studies of their composition, structural, mechanical and tribological properties.

Abbreviations: CNS, carbon nanostructures; PAA, porous anodic alumina; OA, oxalic acid; MA, malonic acid; PA, phosphoric acid; PC, personal computer; CVD, chemical vapour deposition; SEM, scanning electron microscopy; AFM, atomic force microscope.

* Corresponding author.
E-mail address: gorokh@bsuir.by (G.G. Gorokh).

https://doi.org/10.1016/j.apsusc.2017.10.117
0169-4332/

2. Experimental

2.1. Specimen preparation

2.1.1. Formation of anodic alumina matrix

Initial specimens were high-purity Al films (99.99%), of thickness 1.0 μm, sputtering-deposited by a dc magnetron method onto the 100-mm polished single-crystal silicon wafers with (100) orientation and *n*-type conductivity (4.5 Ω cm). The use of the silicon wafers was essential for providing a flat, electronically isolating substrate surface to support the films and for preparation of film sections for scanning electron microscopy and tribological studies. Schematic diagram reflecting the main steps for forming of anodic alumina matrixes with embedded carbon nanostructures is shown in Fig. 1a.

Sputter-deposited Al layers onto a Si substrate (Fig. 1a$_1$) were anodized in 0.4 mol dm^{-3} aqueous electrolytes of oxalic acid (OA), malonic acid (MA) and phosphoric acid (PA) under potentials of 40 V, 90 V and 150 V, respectively (Fig. 1a$_2$). These electrolytes were chosen because they give formation voltages ranging from roughly 35–160 V. As the voltage determines the size of the oxide cells, the interpore center-to-center distance is in the range of 90–400 nm, while the pore size could be tailored between 30 and 180 nm. Geometrically, these parameters seem to be most compatible for synthesis carbon nanostructures into the pores of alumina. A Keysight programmed dc power supply N5752A controlled by LabVIEW software via PC and a GPIB interface was used as the anodizing unit. To enlarge the pores and increase the surface-to-volume ratio in the alumina films, the as-anodized samples were subjected to pore-widening treatment in 20 g/L CrO_3/35 mL/L H_3PO_4 solution kept at 60 °C hereafter "selective etchant" [8] over various periods of time lasting 3–12 min (Fig. 1a$_3$). As a result, the anodic alumina layers thickness of ~1.2 μm have pore diameters of ~45 nm in the OA, ~95 nm in the MA and ~160 nm in the PA. Fig. 1b shows electron microscopic images of matrixes cross-sections intended for the carbon nanostructures deposition and prepared in oxalic acid (OA template on Fig. 1b$_1$), malonic acid (MA template on Fig. 1b$_2$) and phosphoric acid (PA template on Fig. 1b$_3$).

2.1.2. Synthesis of carbon nanostructures

The carbon nanostructures arrays were synthesized by the atmospheric pressure chemical vapour deposition (CVD) method by means of a high temperature pyrolysis of ferrocene/xylene (feeding) solution at atmospheric pressure using of a matrix PAA as a template for CNS growth. Argon was used as a gas-carrier. The feeding solution was delivered into the synthesis zone by the dosed injection. The advantages of the injection process are that it enables variation of the type of hydrocarbon, percentage content of catalyst in the solution, does not require an additional step of annealing in order to obtain highly uniform distribution of catalyst nanoparticles [9]. In this case, regardless whether catalyst particles are localized at the pores walls of the PAA or at their bottoms. CNS^s are growing from these particles and the geometrical parameters of pore determine the length and diameter of these structures. The synthesis process was realized in the tubular type quartz reactor of the specially constructed equipment [10].

A lot of investigations have been done to find optimal regimes of selective growth of CNS arrays in the PAA. In result of multifactor experiment by using the number of the gas-dynamical parameters such as the rate of injection of the feeding solution into the reaction zone (1–100 cm^3 min^{-1} C_8H_{10}), the rate of gas-carrier flow (100–300 cm^3 min^{-1}), the concentration of catalyst source in the feeding solution (0,5%–10% $Fe(C_2H_5)_2$), the temperature of the synthesis process (1050 K–1150 K), the most homogeneous growth of carbon nanostructures in the pores of different PAA were obtained at T = 1150 K in the environment of N_2 – 225 cm^3 min^{-1} and NH_3 – 75 cm^3 min^{-1} at a flow rate of xylene of 0,16 cm^3 min^{-1} with 1% $Fe(C_2H_5)_2$ during 5 min. N_2 was used as carrier gas. HN_3 was used as an additive gas that activated the inner surface of the anodic alumina pores, on which carbon atoms were deposited as a result of the hydrocarbons pyrolysis and carbon nanostructures grew. The PAA matrices prepared in various electrochemical conditions were used for the CNS synthesis under optimal CVD modes. Fig. 1c shows electron microscopic images of matrices cross-sections with the carbon nanostructures embedded into the pores of OA oxide (Fig. 1c$_1$), MA oxide (Fig. 1c$_2$) and PA oxide (Fig. 1c$_3$).

2.2. Specimen characterization

2.2.1. Scanning electron microscopy

Scanning electron microscopy (SEM) was used to observe the morphology of sections and surfaces of the alumina films with and without CNS. SEM observation was performed in a Hitachi S-806 instrument operated at 20 kV. A layer of gold, less than 5 nm thick, was evaporated onto the sections and surfaces before introducing the specimens into the microscope chamber to reduce charging effect. The surface area occupied by CNS in the anodic films was evaluated using NT-206 atomic force microscope (AFM).

2.2.2. Auger electron spectroscopy

Auger profiles PAA matrices with the CNS were investigated in electron spectrometer equipped with an electron analyzer-type cylindrical mirror [11]. The energy of the probe electron beam was 3 keV, the modulation voltage – 5 V. Auger peak intensity dN/dE for the respective chemical elements (aluminum, carbon, and oxygen) was measured at a modulating voltage of 2.5 V in the energy range of 30–600 eV, registering Auger following characteristic lines: 51 eV – LMM transition in an oxidized aluminum; 68 eV – LMM transition in metallic (non-oxidized) aluminum; 272 eV – KLL transition in carbon; 510 eV – KLL transition in oxygen [12]. Profiling was performed using ion etching of the samples by Ag^+ ion beam with energy of 2 keV. Calculation of the integral content of the main chemical elements in the investigated PAA matrixes was performed according to the procedure described in [13].

2.2.3. Raman spectroscopy

The composition of carbon nanotubes was examined by Raman spectroscopy (RS) using a spectrometer "SPECTRA PRO 500" (Acton, England) with an excitation wavelength of 532 nm and power of 25 mW. The spectrometer "SPECTRUM PRO 500" (25 mW) is set the sensitivity threshold no less than 0.1% (by weight) of carbon nanotubes in KBr, which excludes possibility of synthesis studies in localized areas of the reactor and the substrates with a small amount of the synthesized carbon blacks (KBr pellet – 700 mg). For these purposes the Raman Spectrometer "SPEX" has been used (Ramalog, USA) having the ability to vary the excitation wave length of 488 nm, 514 nm and 647 nm at a power of 60 mW with ability of sensitivity calibration to atmospheric oxygen content.

2.3. Tribological researches

2.3.1. Nanoscratch testing

The Nano-scratch test of the investigated materials was carried out using a commercial Nano-Scratch Tester (NST) CSM Instruments equipped with friction table, with the end radius sphero-conical diamond indenter with a radius of 2 μm. The investigations were performed at room temperature in multi-pass (3-scan) mode (pre-scan – scratch – post-scan) determining profile *P*, depth of scratch D_1, and depth after scratch D_2, respectively. The scratch test was performed in load progressive mode with following parameters: begin test load 0.1 mN, maximum test load 50 mN, loading rate 0.17 mN/s of, horizontal speed 1.7 μm/s and scratch

length 0.5 mm. The applied load in pre-scan and post-scan tests was 0.1 mN. The tests ware repeated at least three times for each sample allowing to obtain average values of required parameters.

2.3.2. Nanoindentation

The nanoindentation test of the investigated materials was carried out using the commercial Ultra Nano Hardness Tester (UNHT) with a diamond Berkovich indenter at room temperature in the Lublin University of Technology (Poland). The main improvements are a new tip and a reference fixing system introduced in Ultra Indenter Head and using active top referencing (very low load applied by the reference – less than 0.01 N), a possibility for depth and load measurements, no temperature effect, feedback loop control of the load applied by the reference and by the indenter, low thermal drift, high resonance frequency, one order less noise level, and a new electronic design.

The nanoindentation tests were carried out using the load-control with linear loading mode, 20 mN/min loading rate and 30 s dwell time. Each sample was measured at 10, 30 and 50 mN of maximum load values. For a given load value five indentations were made and the average values of parameters such as hardness or indentation modulus were calculated. Optical microscopy with CCD camera was used to image selected impression marks.

The indentation modulus H was computed using the standard relation

$$H = F_m/A \tag{1}$$

where F_m is the maximum test load and A projected contact area.

The plane strain modulus E_p is calculated from the Oliver & Pharr method [14] and is given by following equation:

$$E_p = \frac{1}{\frac{1}{E_r} - \frac{1-\nu_i^2}{E_i}} \tag{2}$$

where E_i is the elastic modules of the indenter (it is 1141 GPa for diamond), $_i$ is the Poisson's ratio of the indenter (0.07 for diamond) and E_r is given by

$$E_r = \frac{S\sqrt{\pi}}{2\beta\sqrt{Ah_c}} \tag{3}$$

where β is the geometric factor of the indenter (it equals 1.034 for triangular), h_c is the contact depth of the indenter with the trample at maximum test force F_m, and S is the contact stiffness expressed by derivative at peak load:

$$S = \left(\frac{dF}{dh}\right)_{\max} \tag{4}$$

where F is the applied force and h is the penetration depth.

3. Results and discussion

3.1. SEM observation

In the process of hydrocarbon pyrolysis the tubular carbonic nanostructures were formed in the pores of the PAA, repeating the shape and geometry of the nanopores. CNS was uniformly distributed over the entire pore length from the bottom to the surface forming on it a thin carbon coating. Fig. 1 (c_1, c_2 and c_3) shows representative SEM images of the cross sections of PAA matrices formed in OA, MA, and PA respectively with grown into the pores carbon nanostructures. The external dimensions of CNS were conformed pore diameters and they were equal to 45 nm for OA, 95 nm for MA and 165 nm for PA. The formed CNS had very narrow size distribution for all types of matrices. The inner diameters of the holes in the tubular nanostructures amounted to roughly third of the outer diameter and were respectively 15, 30 and 50 nm. The investigated nanocomposite is an array of the closely packed hexagonal oxide cells with the tubular carbon nanostructures within the pores. On the surface of such structure is covered with a thin dense carbon film about 50 nm thick, the surface of which is an agglomeration of hemispheres. Fig. 2 shows the schematic 3-D images of the structure of the nanocomposite PAA/CNS (Fig. 2a, b) with the defined parameters of the structural elements. The image of the carbon coating on the alumina surface obtained on an atomic force microscope is shown on Fig. 2c. Fig. 2d shows the measured parameters and the calculated data on the microstructure of initial anodic alumina and synthesized nanostructures in the pores of corresponding matrixes.

3.2. Composition of the coatings

The composition of carbon nanostructures in PAA investigated using the Raman spectroscopy. The Raman spectrum shows two bands at 1600 cm^{-1} and 1345 cm^{-1} (Fig. 3a). First indicates that the resulting structures are multiwall carbon nanotubes, corresponding to the double degenerate deformation vibrations of a six-membered ring in E_{2g} electronic configuration D^4_{6h} crystal symmetry, indicating that multiwalled structure nanotubes on the PAA matrix surface [15]. The second band at 1345 cm^{-1} corresponds to the vibrational states of the broken hexagonal crystal lattice near the boundary and indicates the presence of amorphous transitional forms of carbon (crushed graphite, carbon black) [16,17].

To study the distribution of concentrations of the major elements of the profile structures from the surface to the silicon substrate, Auger analysis of the samples was performed (Fig. 3b). The spectrum shows the changes in concentrations of the major elements (aluminum – Al, oxygen – O, carbon – C, silicon – Si) in matrix of PAA with CNS. On the surface structure the C concentration is the highest, which is associated with CNS and nanometer thin carbon layer covering the surface of the porous matrix (see Fig. 1), the thickness of which can be up to 50 nm. At the depth of 40–50 nm from the surface the C appear as partial structure of the oxide. Concentrations of O and Al remain approximately constant throughout the thickness of the oxide; C concentration also remains constant, which indicates the formation of carbon-containing tube that is located along the length of the pores [18]. At the bottom of pores the carbon concentration has decreased. Since the approach of carbon concentration to zero, on the spectrum the concentration of Si begins to appear, its concentration increases sharply with advancing inland. Silicon appears well before the front reaches the etching of the silicon substrate. The overlap concentration suggests that the carbon nanostructures and the silicon substrate form a carbide compound.

Important information from the Auger analysis is the ratio of the concentrations of atoms Al, O and C. So, in the usual Al_2O_3 concentration ratio of Al and O is 2/3, which is equivalent to 40% Al to 60% O. After synthesis of CNS concentrations of Al and O reduced to 29% and 52% respectively. This may be due to the fact that during the high-temperature synthesis on the inner surface of the pore walls there is a restoration of Al and O oxide by carbon, and oxygen escapes, and aluminum combined with carbon form a carbide compound Al_4C_3 [18]. This is also confirmed by the data obtained using SEM, since the diameters of carbon nanostructures by 10–15 nm larger of pore diameters of initial PAA matrixes.

3.3. Scratch testing of carbon composite coatings

Fig. 4 shows the dependences of the friction force and friction coefficient (Fig. 4a), and the penetration depth of a cantilever into the three different types of anodic alumina films of the applied load to the cantilever (Fig. 4b). It is shown that the dependences of the

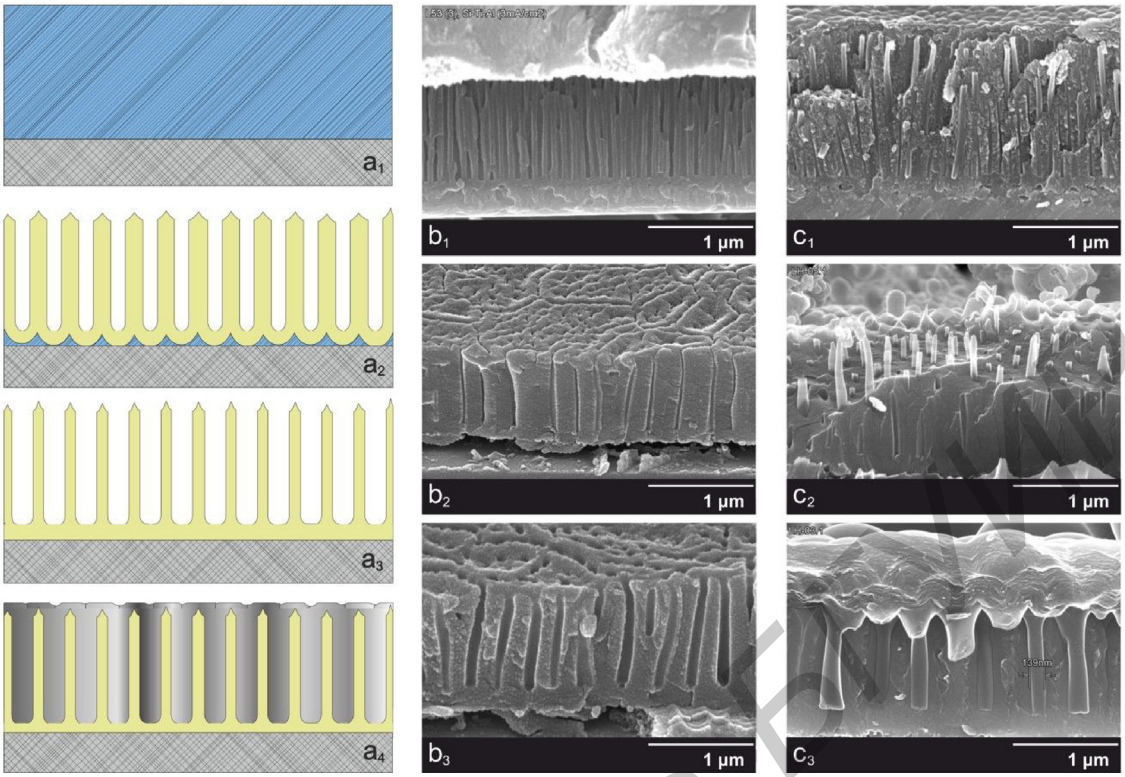

Fig. 1. A – Schematic diagram showing the main steps for forming of PAA matrixes with embedded carbon nanostructures: (a_1) – sputter-deposition of an Al layer onto a Si substrate, (a_2) – anodizing the Al layer to form PAA film, (a_3) – the pore widening treatment of anodic alumina, (a_4) – the synthesis of carbon nanostructures in the pores of PAA. B – Images of PAA matrixes formed in solutions of OA (b_1), MA (b_2) and PA (b_3). C – Images of PAA matrixes with carbon nanostructures grown into the pores of OA (c_1), MA (c_2), and PA (c_3).

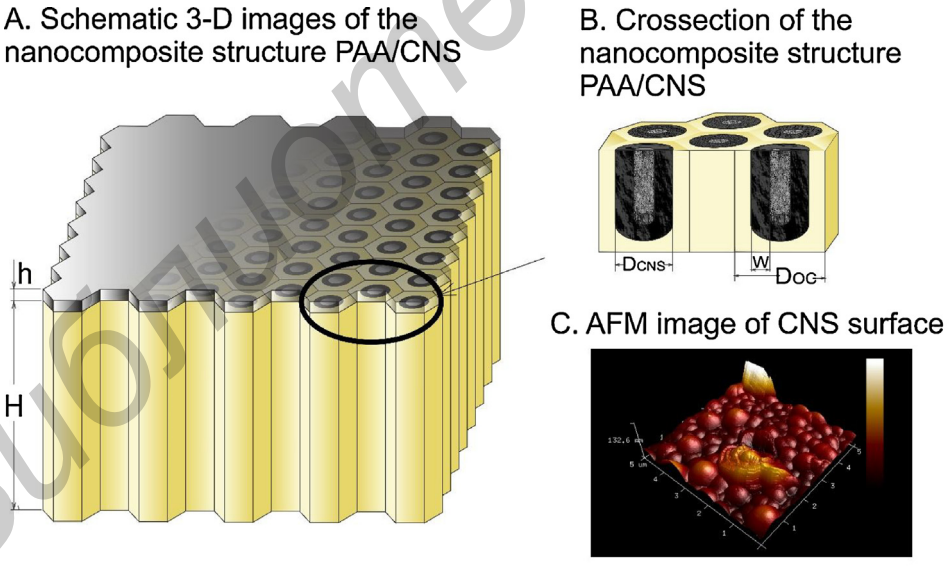

D. Parametres of structural elements of nanocomposite PAA/CNS

Sample	D_{OC}, nm	D_{CNS}, nm	W, nm	H, um	h, nm	N, cm^{-2}
OA	102	45	15	1,5	50	$1,2 \cdot 10^9$
MA	230	95	30	1,25	50	$5,2 \cdot 10^8$
PA	382	150	50	1,45	50	$2,4 \cdot 10^8$

Fig. 2. Schematic 3-D images of the nanocomposite structure PAA/CNS (A, B) with defined parameters of structural elements, AFM image of the carbon coating (C) and the table of structural elements nanocomposite parameters for the different types of PAA (D): where H – the PAA thickness; h – the thickness of the carbon coating on the oxide surface; D_{OC} – the diameter of PAA oxide cell, D_{CNS} – the diameter of CNS; W – the wall thickness of CNS; N – packaging density of oxide cells with CNS in the pores of PAA.

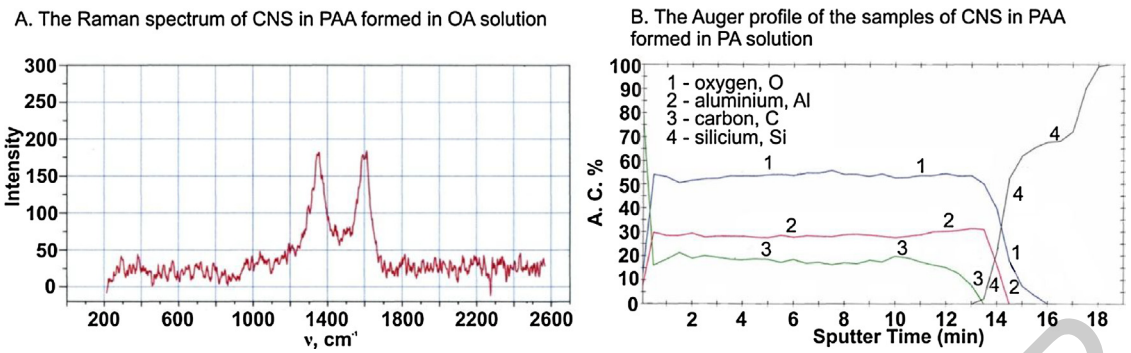

Fig. 3. A – the Raman spectrum of CNS in PAA formed in OA solution; B – the Auger profile of the samples of CNS in PAA formed in PA solution.

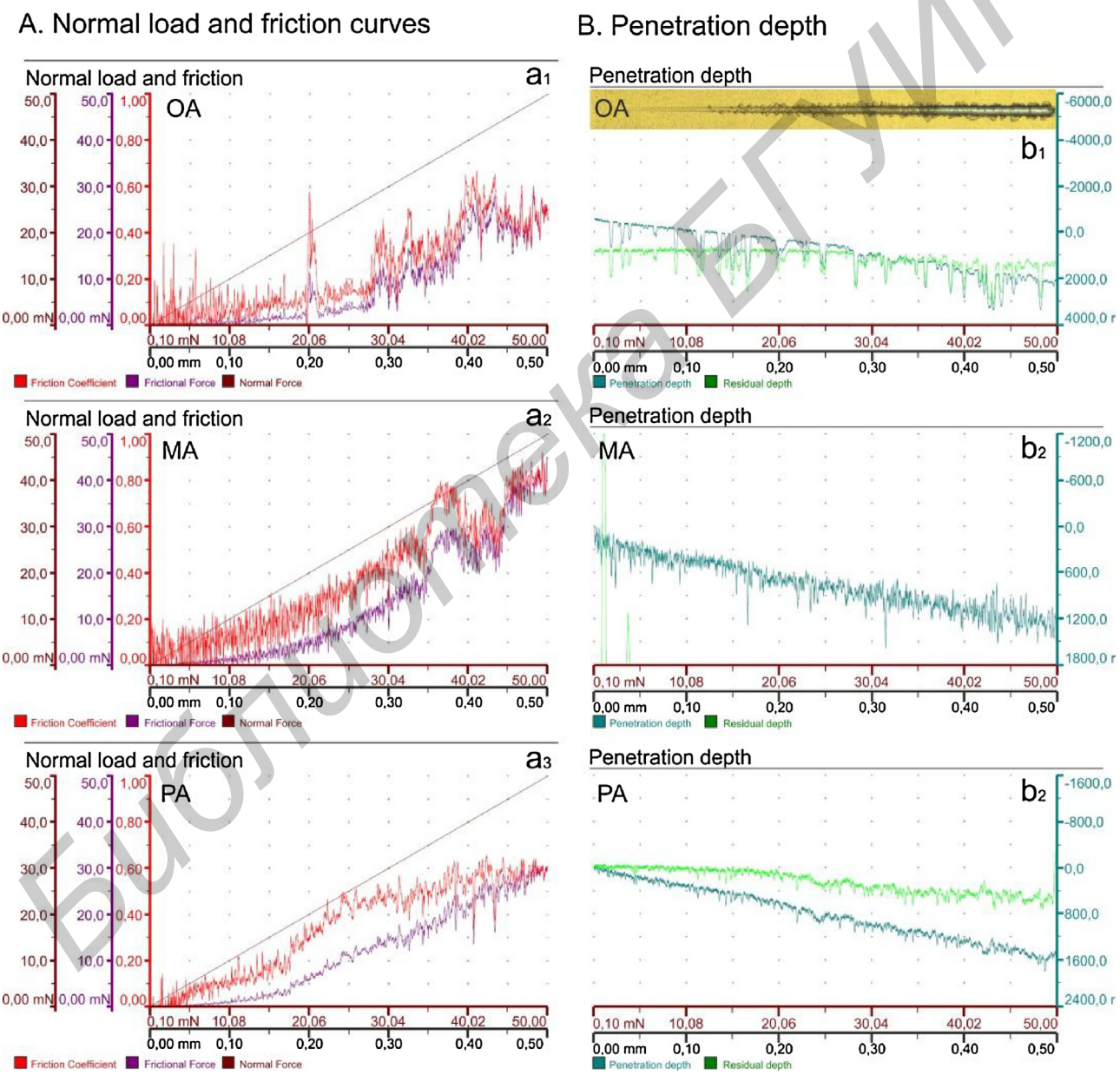

Fig. 4. Typical normal load and friction curves (A) and penetration depth during scratch testing (B) of PAA matrixes with carbon nanostructures grown into the pores formed in OA, MA, and PA. Inset: Example of scratch produced on the surface of OA sample.

friction coefficient of the applied load are nonlinear for all the samples, in addition the measured friction coefficients vary only slightly under loads up to 20 mN. It has been established that the composite films based on OA-alumina with smallest pore diameter and CNS of 45 nm (see table on Fig. 2) have the least friction coefficient at the maximum load, and with the increasing in CNS diameters

Table 1
The main characteristics of composite films by nanoindentation.

Sample	Load P_{max}, mN	Penetration depth h, nm	Hardness H, MPa	Strain modulus E_p, GPa
OA	50	555	5882,3	71,3
	30	475	2605,2	49,6
	10	380	2495,4	46,1
MA	50	920	5102,7	72,5
	30	780	2284,2	54,4
	10	445	2141,4	61,3
PA	50	1235	7128,4	53,1
	30	950	1602,2	39,3
	10	820	631,7	14,9

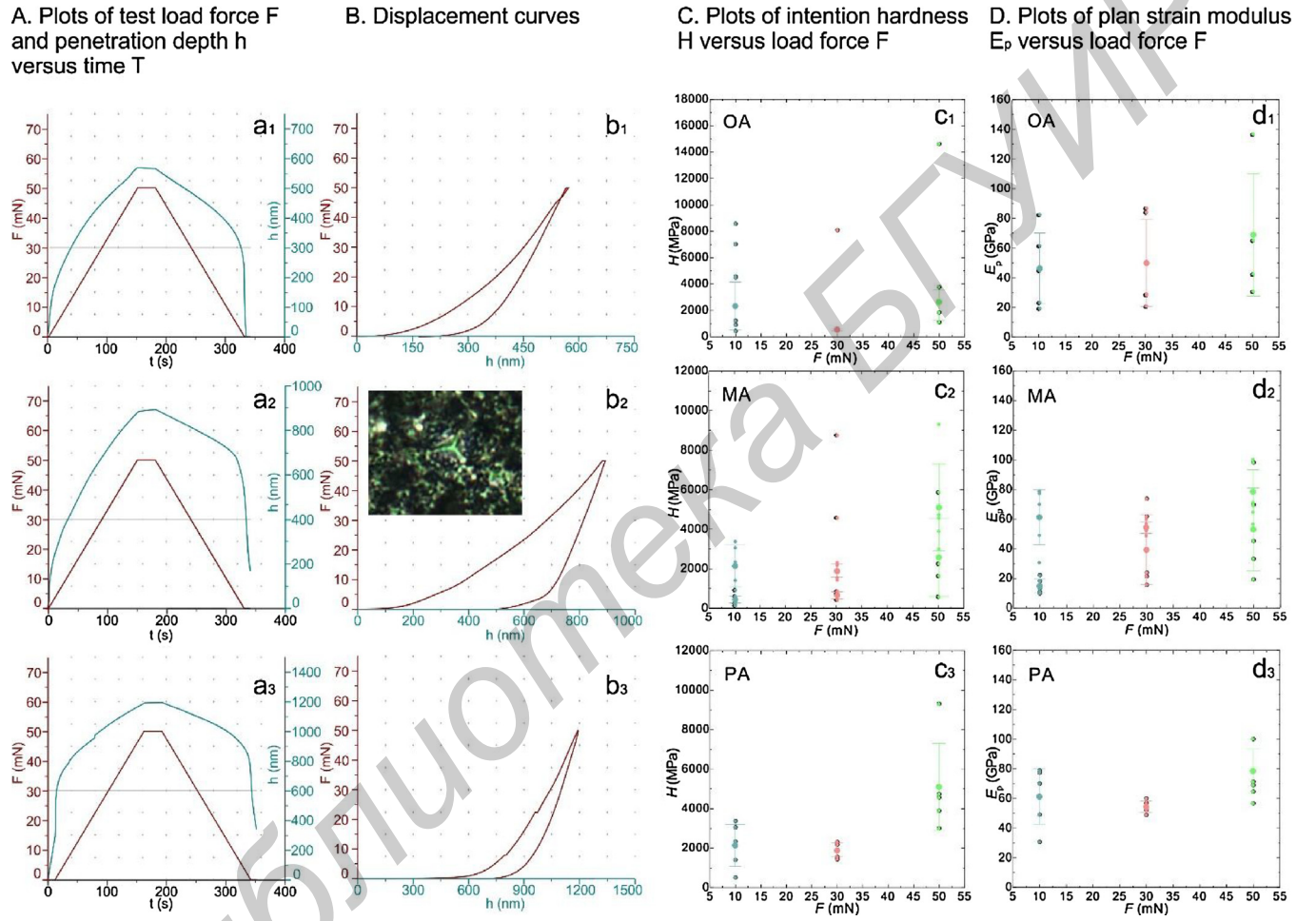

Fig. 5. (A) – typical plots of test load force and penetration depth versus time; (B) load–displacement curves measured during nanoindentation of CNS/PAA matrixes with carbon nanostructures grown into the pores formed in OA, MA, and PA. Inset: Example of nanoindentation imprint made at 50 mN test load produced on surface of MA sample. (C) – Plots of intention hardness *H* versus load force *F* of (c_1) OA, (c_2) MA and (c_3) PA samples; (D) - plots of plan strain modulus E_p versus load force *F* of (d_1) OA, (d_2) MA and (d_3) PA samples.

the friction coefficients are growing. These results showed a high mechanical strength of the carbon-oxide composite films. Thus for OA-sample at the maximum load of 50 mN on the diamond needle of 2 μm in diameter the penetration depth did not exceed of 20% of 1.5 μm film after the first pass, and 40% after the sixth pass.

3.4. Nanoindentation of carbon composite coatings

Fig. 4a shows the kinetics of penetration depth of diamond Berkovich indenter into the PAA matrixes upon loading of indenter up to P_{max} of 50 mN at 20 mN/min, holding for 30 s, and subsequent unloading. The load–displacement curves measured during nanoindentation of OA, MA, and PA matrixes with CNS are given in Fig. 5b. The average microhardness and modulus of elasticity after quintuple studies of each sample (Fig. 5c,d) were calculated according to the formula (1) by the Oliver-Farr technique [14], the obtained values of these quantities are represented in Table 1.

The data show that the microgeometry of nanostructured films has an impact on the value of the microhardness (H), so H values decrease with increasing of CNS diameters. However, in the case of the PA-sample having the pore size of about 150 nm the H value at Pmax = 50 mN substantially exceeds microhardness for the remaining samples. This is related to the penetration of indenter through the border film/substrate interface. If the indenter does not

reach the film/substrate interface, the plastic deformation caused by the penetration of the indenter into the sample is mainly localized within the film. As a result, the measured microhardness value reflects the response of the film material. When the indenter breaks through the interface film/substrate the silicon substrate deformation begins. In its turn, it causes the sharp rise in the PA-sample hardness up to the values tending to the substrate hardness.

Thus, summing up the above, it should be noted that the detected pattern – the microhardness of the samples representing the matrix films with the vertically oriented tubular nanostructures of carbon material increases with diminishing of the oxide cell diameters in series alumina's PA-MA-OA. The depth of the penetration of cantilever into the film conversely grows with the increase of the diameter of the nanostructures in the following order OA-MA-PA oxides. The elastic modulus features have a more complicated dependence and they are increasing in the following sequence of oxides PA-OA-MA.

4. Conclusions

Nanoporous alumina templates were prepared by anodizing Al films on *n*-type Si wafers in 0.4 M oxalic acid (OA template), malonic acid (MA template) and phosphoric acid (PA template) and subjected to chemical pore widening. The carbon nanostructures were synthesized by means of a high temperature pyrolysis of ferrocene/xylene (feeding) solution at atmospheric pressure into the pores of all PAA. The carbon nanostructures completely filled the pores of templates and uniformly covered the tops. The structure of carbon nanostructures corresponded to the structure of multiwall carbon nanotubes. Investigations of mechanical and tribological properties of nanostructured oxide-carbon composite performed by scratching and nanoindentation showed nonlinear dependencies of the frictional force, penetration depth of the cantilever with linearly increasing loads at the end of the cantilever from 0.1 to 50 mN at 1 mN/s, and so the hardness and plane strain modulus on the load. It was found that the microhardness of the samples was increased with reduction of alumina pore diameter, and the penetration depth of the cantilever into the film was grown with increase of CNS size.

Thus, the nanostructured oxide-carbon composite based on nanoporous anodic alumina with embedded tubular carbon nanostructures have high tribological and mechanical properties as well as great practical value. Techniques of forming of spatially ordered nanocomposite matrix carbon containing coatings using porous anodic alumina matrixes can be easily integrated into the standard technology, and allow the forming of functional coatings with the reproducible properties, the precisely controlled thickness and microstructure on products with arbitrary shape.

This research did not receive any specific grant from funding agencies in the public, commercial, or not-for-profit sectors.

References

[1] A. Agarwal, S.R. Bakshi, D. Lahiri, Carbon Nanotubes: Reinforced Metal Matrix Composites, CRC Press, Boca Raton, 2010.
[2] B. Liu, L.R. Liu, X.J. Liu, Effects of carbon nanotubes on hardness and internal stress in Ni–P coatings, Surf. Eng. 29 (7) (2013) 507–510.
[3] M. Pashechko, K. Lenik, Segregation of atoms of the eutectic alloys Fe–Mn–C–B–Si–Ni–Cr at friction wear, Wear 267 (2009) 1301–1304.
[4] Y. Lei, W. Cai, G. Wilde, Highly ordered nanostructures with tunable size, shape and properties: A new way to surface nano-patterning using ultra-thin alumina masks, Prog. Mater. Sci. 52 (4) (2007) 465–698.
[5] G. Gorokh, A. Mozalev, D. Solovei, V. Khatko, E. Llobet, X. Correig, Anodic formation of low-aspect-ratio porous alumina films for metal-oxide sensor application, Electrochim. Acta. 52 (4) (2006) 1771–1780.
[6] V. Khatko, G. Gorokh, A. Mozalev, D. Solovei, E. Llobet, X. Vilanova, X. Correig, Tungsten trioxide sensing layers on highly ordered nanoporous alumina template, Sens. Actuators B: Chem. 118 (1-2) (2006) 255–262.
[7] Z. Cheng, L. Sun, Z.Y. Li, P. Serbun, N. Kargin, V. Labunov, B. Shulitski, I. Kashko, D. Grapov, G. Gorokh, Field emission cathodes based on structured carbon nanotube arrays, World J. Res. Rev. 4 (3) (2017) 8–27.
[8] V. Khatko, A. Mozalev, G. Gorokh, D. Solovei, F. Guirado, E. Llobet, X. Correig, Evolution of surface morphology and crystal texture of WO3 layers sputtered onto Si-supported nanoporous alumina templates, J. Electrochem. Soc. 155 (7) (2008) K116–K123.
[9] V.A. Labunov, B.G. Shulitski, A.L. Prudnikava, Y.P. Shaman, A.S. Basaev, The effect of gas-dynamic factors on selective carbon-nanotube synthesis by injection CVD method for field-emission cathodes, J. Soc. Inf. Disp. 17 (5) (2009) 489–495.
[10] A. Saurov, A. Basaev, V. Labunov, B. Shulitski, A. Pavlov, A. Prudnikava, Y. Shaman, V. Galperin, inventors; Federal State Founding Scientific Production Cpmplex 'Technological Center' of the Moscow State Institute of Electronic Engineering, assignee. Equipment for carbon nanostructures synthesis. Eurasian Patent B82 B 3/00 (2006.01), D01F 9/133 (2006.01)/№ 015412. 2011 Aug 30.
[11] M.P. Seah, D. Briggs, Practical surface analysis Auger and X-Ray Photoelectron Spectroscopy, Vol. 1, 2nd ed., Wiley & Sons, Chichester, 1995.
[12] L.E. Davis, N.C. MacDonald, P.W. Palmberg, G.E. Riach, Handbook of Auger Electron Spectroscopy, Perkin-Elmer Corp, Eden Prairie, 1978.
[13] P. Weightman, The development of auger spectroscopy as a probe of local electronic structure, Microsc. Microanal. Microstruct. 6 (3) (1995) 263–288.
[14] W.C. Oliver, G.M. Pharr, Improved technique for determining hardness and elastic modulus using load and displacement sensing indentation experiments, J. Mater. Res. 7 (6) (1992) 1564–1583.
[15] L. Valentini, L. Lozzi, C. Cantalini, I. Armentano, J.M. Kenny, L. Ottaviano, S. Santucci, Effects of oxygen annealing on gas sensing properties of carbon nanotube thin films, Thin Solid Films 436 (1) (2003) 95–100.
[16] M.J. Kim, T.Y. Lee, J.H. Choi, J.B. Park, J.S. Lee, S.K. Kim, J.B. Yoo, C.Y. Park, Growth of carbon nanotubes with anodic aluminum oxide formed on the catalytic metal-coated Si substrate, Diam. Relat. Mater. 12 (3) (2003) 870–873.
[17] A.C. Dillon, A.H. Mahan, J.L. Alleman, M.J. Heben, P.A. Parilla, K.M. Jones, Hot-wire chemical vapor deposition of carbon nanotubes, Thin Solid Films 430 (2003) 292–295.
[18] S. Mercier, P. Ehrburger, J. Lahaye, Interfacial reactivity in aluminium/carbon fibre composites, J. Phys. IV 3 (1993) 1723–1726.